Journal of
BIOPHOTONICS

FULL ARTICLE

Vibrational spectroscopic imaging and live cell video microscopy for studying differentiation of primary human alveolar epithelial cells

Branko Vukosavljevic[1,2] | Marius Hittinger[1,2] | Henning Hachmeister[3] | Christian Pilger[3] | Xabier Murgia[1] | Michael M. Gepp[4] | Luca Gentile[4] | Hanno Huwer[5] | Nicole Schneider-Daum[1] | Thomas Huser[3] | Claus-Michael Lehr[1,2,6] | Maike Windbergs[1,2,7]*

[1]Helmholtz Institute for Pharmaceutical Research Saarland (HIPS), Helmholtz Centre for Infection Research (HZI), Saarland University, Saarbrücken, Germany

[2]PharmBioTec GmbH, Saarbrücken, Germany

[3]Biomolecular Photonics, Faculty of Physics, Bielefeld University, Bielefeld, Germany

[4]Fraunhofer Institute for Biomedical Engineering IBMT, Sulzbach, Germany

[5]Heart and Thoracic Surgery, SHG Kliniken Völklingen, Saarbrücken, Germany

[6]Department of Pharmacy, Saarland University, Saarbrücken, Germany

[7]Institute of Pharmaceutical Technology and Buchmann Institute for Molecular Life Sciences, Goethe University Frankfurt, Frankfurt am Main, Germany

*Correspondence
Maike Windbergs, Institute of Pharmaceutical Technology and Buchmann Institute for Molecular Life Sciences, Goethe University Frankfurt, Max-von-Laue-Str. 15, 60438 Frankfurt am Main, Germany.
Email: windbergs@em.uni-frankfurt.de
Claus-Michael Lehr and Nicole Schneider-Daum, Helmholtz Institute for Pharmaceutical Research Saarland (HIPS), Helmholtz Centre for Infection Research (HZI), Saarland University, Campus E8 1, 66123 Saarbrücken, Germany.
Email: Claus-michael.lehr@helmholtz-hzi.de; nicole.daum@helmholtz-hzi.de

Alveolar type II (ATII) cells in the peripheral human lung spontaneously differentiate toward ATI cells, thus enabling air-blood barrier formation. Here, linear Raman and coherent anti-Stokes Raman scattering (CARS) microscopy are applied to study cell differentiation of freshly isolated ATII cells. The Raman spectra can successfully be correlated with gradual morphological and molecular changes during cell differentiation. Alveolar surfactant rich vesicles in ATII cells are identified based on phospholipid

vibrations, while ATI-like cells are characterized by the absence of vesicular structures. Complementary, CARS microscopy allows for three-dimensional visualization of lipid vesicles within ATII cells and their secretion, while hyperspectral CARS enables the distinction between cellular proteins and lipids according to their vibrational signatures. This study paves the path for further label-free investigations of lung cells and the role of the pulmonary surfactant, thus also providing a basis for rational development of future lung therapeutics.
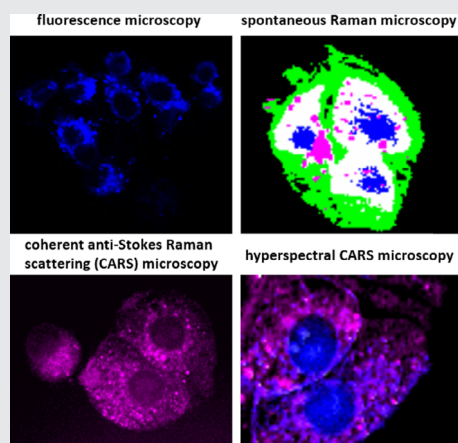
KEYWORDS

CARS microcopy, cell imaging, confocal laser scanning microscopy, confocal Raman microscopy, pneumocyte type II differentiation

1 | INTRODUCTION

The alveolar epithelium of the peripheral human lung is mainly composed of two cell phenotypes: alveolar type I (ATI) cells capable of forming a cellular barrier towards the respiratory tract and ATII cells responsible for production, accumulation and secretion of alveolar surfactant lining the cells in the deep lung. At the same time, ATII cells function as progenitors for the ATI cell phenotype. Differentiation of ATII cells to ATI cells is accompanied by drastic morphological and molecular modifications, especially with respect to the cellular lipid content and expression of specific marker proteins (ie, surfactant protein C [SP-C] and caveolin-1) [1–5]. After differentiation, the ATI cells allow for the in vivo gas exchange and cover more than 90% of the alveolar surface area.

The morphological and structural changes occurring on differentiation of ATII cells have already been visualized by scanning electron microscopy and transmission electron microscopy [1, 6], these techniques are, however, operating in vacuum and lack chemical selectivity. Expression of typical markers, for example, surfactant proteins (SP-C, SP-A and so on) and caveolin-1 have been investigated with confocal laser scanning microscopy, reverse transcriptase polymerase chain reaction, flow cytometry and immunoblotting [1, 7]. However, these methods require the fixation and/or disruption of the cells under investigation [8, 9]. Consequently, to study the surfactant secretion and accompanied cellular differentiation in an unperturbed environment and without influencing cellular membranes, we applied noninvasive and label-free analytical approaches to expand and complement the current knowledge in the field [10].

In this context, vibrational spectroscopic techniques represent an upcoming approach for label-free visualization of cells and their changes based on subtle spectral changes which can be correlated with molecular changes. Major techniques based on this concept are confocal Raman microscopy (CRM) and coherent anti-Stokes Raman scattering (CARS) microscopy, which unlike infrared microscopy allow for in vitro analysis in aqueous media [11]. A Raman spectrum of a cell represents an intrinsic biochemical fingerprint, containing molecular-level information about cellular biopolymers, including DNA, RNA, proteins, lipids and carbohydrates [12]. Moreover, because CRM as a linear technique also allows for quantification of chemical components based on peak intensities, such spectra are sensitive to changes in molecular composition and can be used as cell-specific biochemical signatures to discriminate between different cellular phenotypes [13–15].

Both, CRM and CARS microscopy, are based on inelastic scattering of the excitation laser light; however in general for CRM, the scattered photons bear less energy compared to the exciting laser light, while for CARS microscopy the contrary correlation applies. The total Raman signal collected from a sample by applying CRM is the incoherent addition of the signals (peaks) from individual molecules, which results in low Raman scattering intensities, and therefore long integration times. In addition, autofluorescence of many biomolecules can hinder the detection of a Raman signal. By applying CARS microscopy, some of these limitations can be overcome, as the total CARS signal arises from the coherent addition of the signals from individual molecules. The resulting CARS signal is up to five orders of magnitude stronger than the corresponding spontaneously Raman scattered signal [16]. Owing to the increased signal intensity, CARS data can be collected even at video-rate, although at very low sample concentrations, the advantages of the coherent addition of the CARS signals from many identical molecular groups is reduced and the presence of the non-resonant background becomes an increasing problem. Altogether, spontaneous and coherent Raman scattering methods represent an emerging complementary platform for label-free and chemically selective cellular imaging [12, 16, 17].

The aim of this study was to biochemically characterize and visualize the in vitro differentiation of primary human alveolar epithelial cells with CRM and CARS microscopy as a label-free approach. We investigated the gradual metamorphosis of ATII into ATI cells and followed the key biochemical changes within the cells undergoing differentiation. Moreover, we applied live cell video imaging to visualize the growth, spread and morphological changes of living cells for up to 6 days in culture and correlated these label-free and non-destructive methods with conventional fluorescence staining.

2 | MATERIALS AND METHODS

2.1 | Isolation and culture of primary alveolar epithelial cells

Lung tissue was received from the Heart Center Voelklingen from patients undergoing lung resection after informed consent from all participants and/or their legal guardians and in compliance with a protocol approved by the Ethics Commission of the "Ärztkammer des Saarlandes" (file number 136/13). All experiments were approved to be performed in accordance with approved guidelines and regulations.

The isolation of primary epithelial cells was based on an established protocol [18]. Briefly, lung tissue was chopped in small cubes and washed three times in balanced salt solution (137 mM NaCl, 5 mM KCl, 0.7 mM Na2HPO4, 10 mM HEPES, 5.5 mM glucose, pH 7.4) using a cell strainer (100 µm pore size; Becton Dickinson, Heidelberg, Germany). A trypsin (Sigma-Aldrich, Deisenhofen, Germany)-elastase (Worthington, Lakewood, New Jersey) solution was used to digest the lung cell suspension in 40 minutes at 37°C. Cells were subsequently incubated in

cell culture petri-dishes to remove tissue macrophages for 90 minutes and remaining erythrocytes were removed with a percoll gradient (Sigma-Aldrich). The ATII cells were isolated from the cell suspension by positive selection with an EPCAM-antibody (Miltenyi Biotec, Bergisch Gladbach, Germany). Cells were seeded on glass slides without any coating and cultured in Small Airway Epithelial Cell Growth Medium—SAGM (Lonza, Verviers, Belgium).

2.2 | Immunocytochemistry (pro-surfactant protein C and caveolin-1 staining)

Cells were grown for 7 days and fixed on glass coverslips with 3% paraformaldehyde solution (30 minutes at room temperature). After incubation with 1% BSA (Sigma-Aldrich) for 30 minutes, cells were stained with two antibodies: anti-prosurfactant protein C marker (anti human, rabbit origin, Merck Millipore, Darmstadt, Germany) for ATII cells which recognizes the Sp-C proprotein as well as processing intermediates and anti-Caveolin 1 marker (anti human, mouse origin Novus Biologicals, Wiesbaden Nordenstadt, Germany) for ATI cells, which recognizes both the α and β isoforms of the protein, to verify the differentiation process (images were acquired on day 1, 2, 3, 5 and 7). Cells were incubated with two primary antibodies during 24 hours at 4°C (1:500 dilution), and with secondary antibodies for 2 hours at room temperature (1:200 dilution). In addition, before imaging, we stained cellular nuclei with DAPI (4′,6-diamidino-2-phenylindole dihydrochloride, 1:50 000 dilution).

2.3 | Laurdan fluorescence staining

We used laurdan (6-lauroyl, 1-2-dimethylamino naphthalene) as a fluorescent probe for the visualization of primary alveolar epithelial cells differentiation, due to the change of lipid content on cell differentiation. The Laurdan molecules possess a dipole moment and detect changes in membrane phase properties due to their sensitivity to the polarity of the environment in the lipid bilayer [19–21]. For the staining of intracellular lipid vesicles with laurdan, primary human ATII cells grown on glass coverslips were incubated with 0.05 μM laurdan in SAGM for 1 hour at 37°C.

2.4 | Confocal fluorescence microscopy

Fixed cells were analyzed by confocal fluorescence microscopy (Zeiss LSM710, Zeiss, Germany). Microscopic images of fixed samples were acquired at either 512×512 pixels or 1024×1024 pixels using a 40× and 63× water immersion objective lens, respectively. Confocal images were analyzed using the Zen 2012 software (Carl Zeiss Microscopy GmbH).

2.5 | Confocal Raman microscopy

Visualization of alveolar surfactant secretion during human epithelial lung cells differentiation was performed using a confocal Raman microscope (WITec alpha 300R$^+$, WITec GmbH, Ulm, Germany). The excitation source was a 532 nm diode laser adjusted to a power of 30 mW in front of the objective and a 50 μm confocal pinhole rejecting signals from out-of-focus regions. A 63× water immersion objective lens with a numerical aperture (NA) of 1.0 (Epiplan Neofluar, Zeiss) was utilized. We analyzed cells from three different human donors to exclude interindividual variations of the cells. Cells were cultured in SAGM medium on Ca-fluoride well plates (50 000 cells/well) and the living cells were imaged in live state during a period of 7 days (for the days 4, 5, 6 and 7, medium was changed once, after 3 days). For acquisition of the reference spectrum, dipalmitoyl phosphatidylcholine (DPPC) was purchased from Avanti Polar lipids, Inc. (Alabaster, Alabama). All acquired Raman spectral data sets were preprocessed by removing cosmic rays and by background signal reduction (second order polynomial fitting), before conversion into false color images using hierarchical cluster analysis (WITec Project Plus software).

2.6 | CARS microscopy

2.6.1 | CARS microscopy setup

CARS microscopy was performed on a home-built laser scanning microscope (Supporting information Figure S1) employing galvanometric scanning mirrors (Galvanometer Optical Scanner, Model 6215H; Cambridge Technology, Bedford, Massachusetts). A frequency-doubled 1064 nm Nd:VAN laser (picoTRAIN High Q laser GmbH, Austria) operating at 80 MHz repetition rate pumps an optical parametric oscillator (OPO) (Levante Emerald, APE, Germany) generating the appropriate wavelengths for CARS microscopy. The spatially and temporally overlapping laser beams were focused into the sample using a 60× water immersion objective lens (UPLANSAPO, NA = 1.2; Olympus, Germany). The total focal power was less than 30 mW to avoid destruction of the biological sample.

For lipid imaging, the pump beam wavelength was tuned to 816.7 nm probing in combination with the 1064 nm Stokes beam the 2845 cm^{-1} CH$_2$ stretching mode, which corresponds predominantly to lipids. The CARS signal occurring at 660 nm was isolated by a filter set comprised of a 950 SP, 775 SP (two times), 785 SP and a 660/40 bandpass filter.

All signals were detected using a photomultiplier tube (PMT) (H 9656–20, Hamamatsu Photonics, Japan) by collecting the photons in forward direction through a condenser lens (Olympus U-AAC, NA 1.4; Olympus). The resulting PMT signal is acquired by an analogue-to-digital (A/D) converter (PCI-6110S; National Instruments, Austin, Texas) and

processed by ScanImage (version 3.8.1, Howard Hughes Janelia Farm Research Campus) [22].

To visualize the cellular volume, we acquired three-dimensional (3D) data sets of the intracellular lipids for one biological replicate per day with a step size of 300 nm in the axial (z) direction by utilizing a piezo-stage (S/N 222009, Märzhäuser, Germany). A full 3D scan contains approximately 30 to 40 images covering the full volume of the cells (diameter 6-12 μm) within the region of interest (ROI). The field of view was 75 × 75 μm for each image (512 × 512 pixels) and was scanned with a pixel dwell time of 31.25 μs resulting in a full acquisition time of approximately 6 minutes per image.

For hyperspectral (HS) image acquisition, the pump beam was tuned for each image with 0.3 nm step size by using a home written MATLAB program which controls the OPO and the scanning program of the microscope. The spectral range spans from 803 to 826.5 nm which corresponds to a vibrational spectrum ranging from 2700 to 3050 cm^{-1}. While scanning the OPO pump wavelength, we control both the LBO crystal's temperature as well as the OPO's cavity length through a mirror mounted on a linear translation piezo stage. Owing to this provision, we ensure that the output power of the OPO as well as the pulse length remains constant. In addition, two photo diodes (PDs) (PDB-C613-2; Luna Optoelectronics, Camarillo, California) record the intensity of Stokes and pump beam for every pixel. In a post-processing step any intensity fluctuation up to 100 kHz can be compensated for based on these data. In case of HS data acquisition the 660/40 nm BP filter was removed from the detection pathway.

2.6.2 | CARS acquisition settings

For CARS microscopy, the focal intensities were set to 10 mW for the Stokes (1064 nm) and 20 mW for the pump beam. For z-stack acquisition the typical pixel dwell time was 31.25 μs with 512 × 512 pixels per image for a field of view covering 75 × 75 μm matching both the size of the cells as well as suitable acquisition times of approximately 6 minutes. In the case of HS CARS we imaged one focal z-position and increased the pixel dwell time to 62.5 μs. The focal position was selected by eye and matched the mid position of the cells in the regions of interest.

2.6.3 | CARS image analysis

The CARS z-scans were intensity corrected with a home-written MATLAB program and analyzed with the image processing software FIJI. The gray scale offset was set to 10% above the background of the image. After that, the plugin "3D-project" was used to arrange all images in a 3D projection. For the final image the 0° angle was selected and presented in the look-up table magenta.

The HS CARS image series was also intensity corrected and processed with custom-written, MATLAB-based

algorithms, which will be highlighted in the following. A HS image series consists of multiple two-dimensional (2D) image sections each displaying a different wavelength combination of pump and Stokes beams. To reduce the influence of arbitrary signal fluctuations we performed a binning step (4 × 4 pixels) on the 2D image sections. Then, a ROI was manually selected typically displaying one or two cells and an offset was subtracted from the image section. Finally, from this ROI four spectra and four image sections were selected and used as initial values for data analysis by the nonnegative matrix factorization (NNMF) algorithm from the MATLAB Statistics toolbox. NNMF is an iterative dimension-reduction method that tries to find two nonnegative matrices W and H with a definite rank number k which represent the original matrix A. Here, k stands for the number of unique vibrational signatures we assumed to be in the image. The algorithm models W and H in such a way that the root-mean-squared residual between A and $W*H$ is minimized [23]. In our case W and H are representing k 2D image sections and vibrational spectra, respectively. Each 2D image section of W corresponds to an intensity distribution of a certain vibrational spectrum of H. Finally, W is then further processed and illustrated with FIJI.

2.6.4 | Live cell video imaging

Long-term observation of the alveolar epithelial cells was conducted under physiological conditions in the automated microscopes Biostation IM-Q (Nikon Instruments Europe BV, Amsterdam, Netherlands). Cells were seeded in collagen/fibronectin-coated petri dishes (35 mm diameter, Corning, New York) in 2 mL cell culture medium and cultivated for 6 days. The cell culture medium was changed twice a week. During cultivation, phase contrast images were acquired at 30-minute intervals at 15 different positions.

3 | RESULTS AND DISCUSSION

The alveolar epithelium of deep lungs comprises two main cellular phenotypes, that is, ATI and type II (ATII) cells. ATII cells act as progenitor cells for ATI cells in the human body, and thus do also spontaneously differentiate into ATI-like cells during in vitro cultivation. This phenomenon is well-known and already reported by several research groups [1–5]. However, a systematic investigation of this cellular metamorphosis and its associated morphological and biochemical changes, including the storage and secretion of the lung surfactant in its unperturbed environment (without labeling or destruction), is still lacking.

We isolated primary human alveolar epithelial cells from lung tissue of patients undergoing lung resection and cultivated them for several days [18]. To visualize surfactant rich vesicular structures, which are typically considered as an indicator for ATII cells, and their gradual disappearance over

time during cell differentiation, we used laurdan as a fluorescence marker for our study. Laurdan allows for detecting time and temperature dependent changes in membrane phase properties by changes of its fluorescence emission spectrum. As presented in Figure 1, individual lipid vesicles could be stained within the cytosol of alveolar epithelial cells (at days 1, 2 and 3) exhibiting a consistent spectral emission of laurdan distributed among ordered lipids (blue). During days 4-7, the differentiation into ATI-like cells was evident by the reduction in the number of cells containing lipid vesicles, as well as in the number of lipid vesicles per cell. Interestingly enough, we were also able to observe some non-differentiating ATII cells in the presence of differentiated ATI-like cells (see white arrow in Figure 1, day 5), supporting the theory that a small number of cells does not act as progenitors for ATI-like cells, but finalizes the cell circle as ATII cells.

Lung surfactant mostly consists of phospholipids, associated with some specific, so-called surfactant proteins of which so far four have been identified (SP-A, SP-B, SP-C and SP-D). The synthesis of the lung surfactant initially occurs in the endoplasmic reticulum (pro-SPC for example), from where it is transported and can finally be localized in lipid vesicles. Those surfactant proteins can be used as significant cellular markers, as they are restricted to the ATII phenotype [24–26]. Moreover, caveolin-1 (cav-1), as a major structural protein of plasma membrane assemblies called caveolae, represents a characteristic feature of ATI-like cells [7, 27, 28]. As additional independent proof of this cellular differentiation process, we applied marker molecules to label SP-C and caveolin-1, and followed the phenotype

change of the cells by confocal fluorescence microscopy, as described by Fuchs et al. (Figure S2) [1]. At days 1, 2 and 3, the expression of pro-SP-C (green), dominates the expression of Cav-1 (red). Over time, at days 5 and 7, pro-SP-C expression dramatically decreases, while Cav-1 expression increases.

While the presented fluorescence images rely on labeling the sample, Raman microscopy techniques allow for label-free imaging based on the spectral cell information comprising content, distribution and concentration of cellular biopolymers (such as DNA, RNA, proteins, lipids and carbohydrates) on the molecular level [12].

Therefore here, we applied CRM to get a non-invasive insight into the differentiation of primary human alveolar epithelial cells which is followed by dramatic changes in the cellular lipid content. To compensate for interindividual variations, we used lung tissues isolated from three different patients. After spectral assignment of the Raman peak patterns, we were able to distinguish the signal contributions of nucleus, cytoplasm, membrane and lipid vesicles characteristic of the ATII phenotype (Figure 2A). The Raman spectrum of lipid vesicles (depicted in pink) was very distinctive, with major contributions by spectral patterns of DPPC. For detailed comparison, both spectra (alveolar surfactant as main component of the lipid vesicles and DPPC as major constituent of the pulmonary surfactant, respectively) are displayed in Figure S3 confirming the localization of alveolar surfactant inside the lipid vesicles [29].

Based on the spectra depicted in Figure 2A, spatially resolved false color images were created for representative cell samples at each day (d1-d7, Figure 2B). Different cell
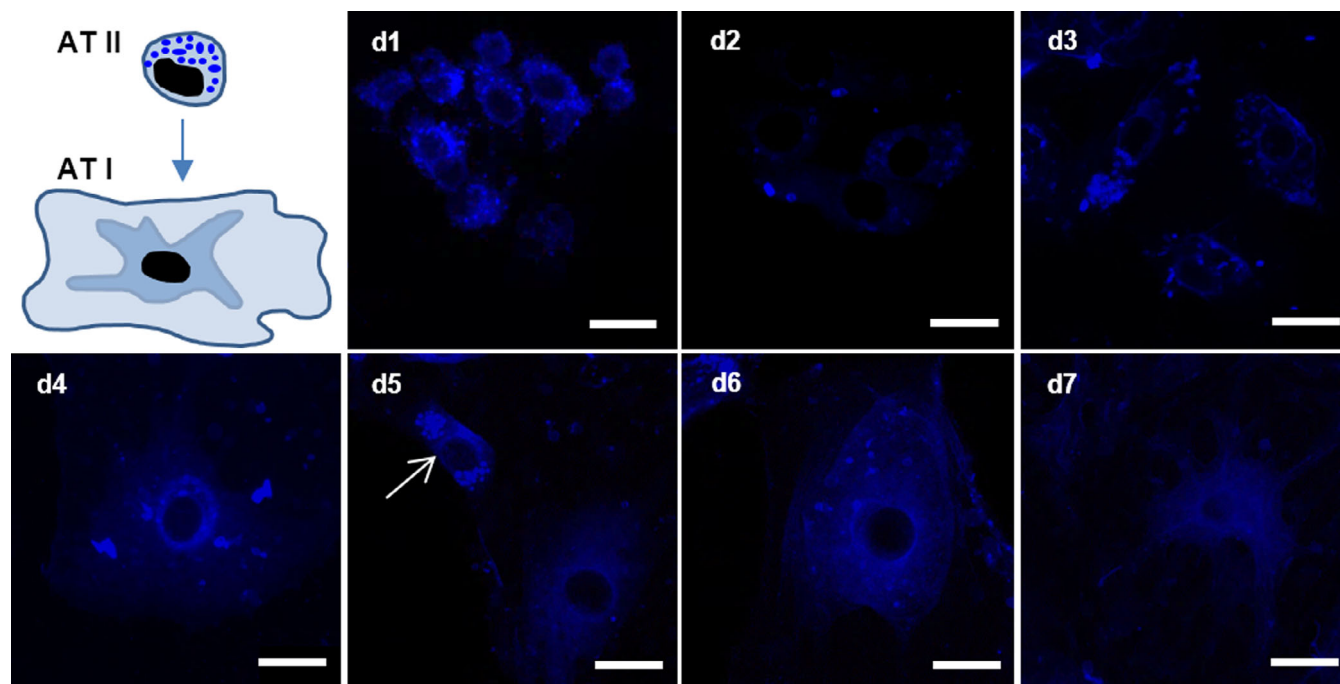
FIGURE 1 Laurdan staining of primary human alveolar epithelial cells from day 1 (d1) to day 7 (d7) visualized by fluorescence microscopy (scale bars 20 μm). The arrow in d5 appoints a non-differentiating surfactant rich alveolar type II (ATII) cell

(A)

(B)
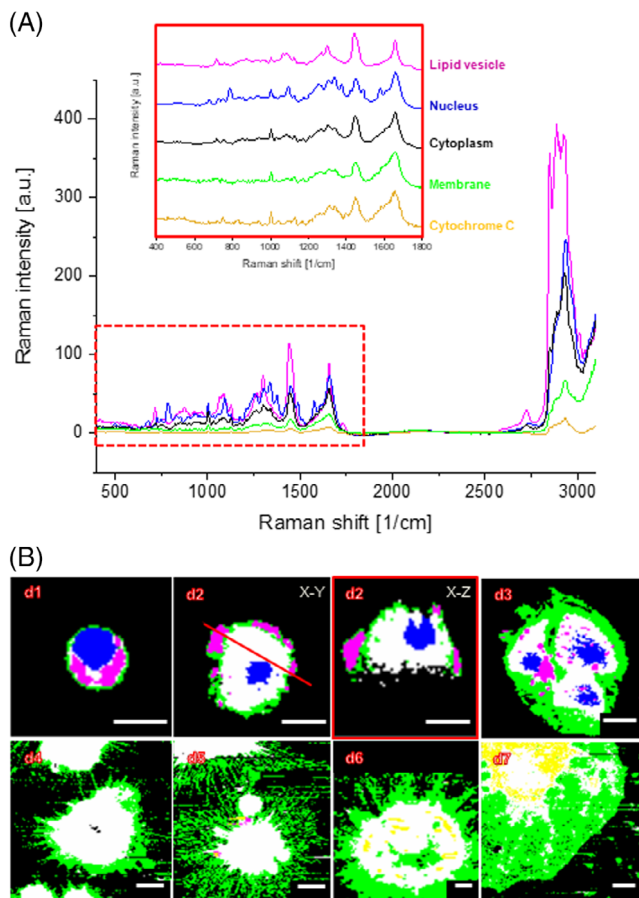
FIGURE 2 Differentiation of alveolar epithelial cells in primary culture visualized by confocal Raman microscopy. A, Raman spectra (full, raw spectra and normalized fingerprint region) of different cellular compartments: lipid vesicles (pink), nucleus (blue), cytoplasm (black), cellular membrane (green) and cytochrome c (yellow), respectively; B, Representative Raman images for days 1 to 7 (d1-d7), respectively. Red line at d2 depicts the focal plane of X-Z cross section presented next to X-Y scan (scale bars 10 μm)

compartments are depicted in individual colors (eg, nucleus-blue, membrane-green, cytosol-white). At day 1 (d1), ATII cells were relatively small (~10 μm in diameter) and cuboidal in shape. Almost the entire cytoplasmic volume was filled with lipid vesicles (pink) in which the alveolar surfactant was deposited. At day 2 (d2), cell growth is clearly visible for ATII cells and the lipid vesicles filled with surfactant can be found close to the cellular membrane or already fused with the membrane for secreting the surfactant (d2, X-Y).
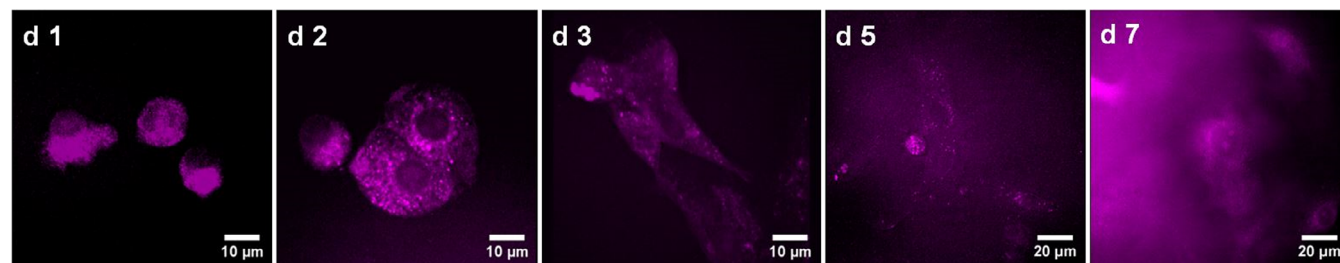
The virtual cross section (d2, X-Z along the red line indicated in d2, X-Y) additionally proved the fusion of lipid vesicles with the cellular membrane, indicating the future secretion into the extracellular environment. Three days after seeding (d3), cells were grouped together forming small islands, and the secretion process was continued. At day 4 and 5 (d4 and d5), no distinct lipid vesicles could be detected any more in the cells, additionally they started exhibiting cellular protrusions, filling the interspaces and thus forming a coherent barrier. Here, it was impossible to visualize the nucleus and, at the same time, the entire cell surface due to the high difference in the thickness between perinuclear region and the periphery. After 6 and 7 days of cultivation (d6 and d7), we detected one characteristic Raman spectrum (depicted in Figure 2A in yellow) exhibiting a band assigned to the tryptophan ring breathing mode within proteins (~757 cm^{-1}). Moreover, the same spectrum displayed a smaller intensity of the Raman band assigned to the nucleic acid backbone and pyrimidine base vibrations (~784 cm^{-1}). As the rapid increase in intensity ratios of Raman bands assigned to the tryptophan and to nucleic acid backbone vibrations is reported to be correlated with cellular differentiation [30], our data corroborate the occurrence of this process in alveolar epithelial cells. In addition, the 750 cm^{-1} peak has been reported to be associated with cytochrome c, a protein released from mitochondria during the process of cellular apoptosis [31]. This observation is in line with the fact that alveolar epithelial cells in primary culture decrease their barrier properties after 7 days. The large green areas attributed to the periphery of differentiated cells showed low scattering intensity (Figure 2A), which is indicative of cellular flattening on the differentiation process.

Furthermore, as observed by laurdan staining in Figure 1, we could also visualize individual ATII cell accompanied by ATI cell at day 3 (representative image in Figure S4), again supporting that some alveolar epithelial cells finalize the cell circle without undergoing such differentiation. Data of repeat experiments for the individual days are depicted in Figure S5.

As mentioned before, on differentiation into ATI-like cells, alveolar epithelial cells dramatically grow and flatten (~2 μm thickness), making their visualization with CRM very challenging. Therefore, we applied CARS microcopy to

FIGURE 3 Coherent anti-Stokes Raman scattering (CARS) images (three-dimensional projections) of alveolar epithelial cells at days 1, 2, 3, 5 and 7, respectively. Bright pink dots represent individual lipid vesicles indicating their intracellular distribution

these samples, which allows for much faster acquisition times and 3D imaging with significantly improved z resolution. Figure 3 depicts the 3D projections of the representative CARS images of alveolar epithelial cells after 1, 2, 3, 5 and 7 days of incubation. Data of repeat experiments for the individual days are depicted in Figure S6, while z-scans on day 1 and 3 are visualized in Figure S7 and S8, respectively.

In addition, a 90° angle projection of alveolar epithelial cells at day 2 confirms the intracellular distribution of lipid vesicles (Figure S9). These images further confirm the previously discussed CRM results (Figure 2).

As an additional investigational approach, we also applied HS CARS imaging. This method combines the two major advantages of linear Raman and CARS microscopy-high chemical selectivity and low acquisition times, respectively. After scanning the samples in the spectral range from 2700 to 3050 cm^{-1}, we used NNMF as a multivariate statistical analysis technique to provide a non-biased spectral
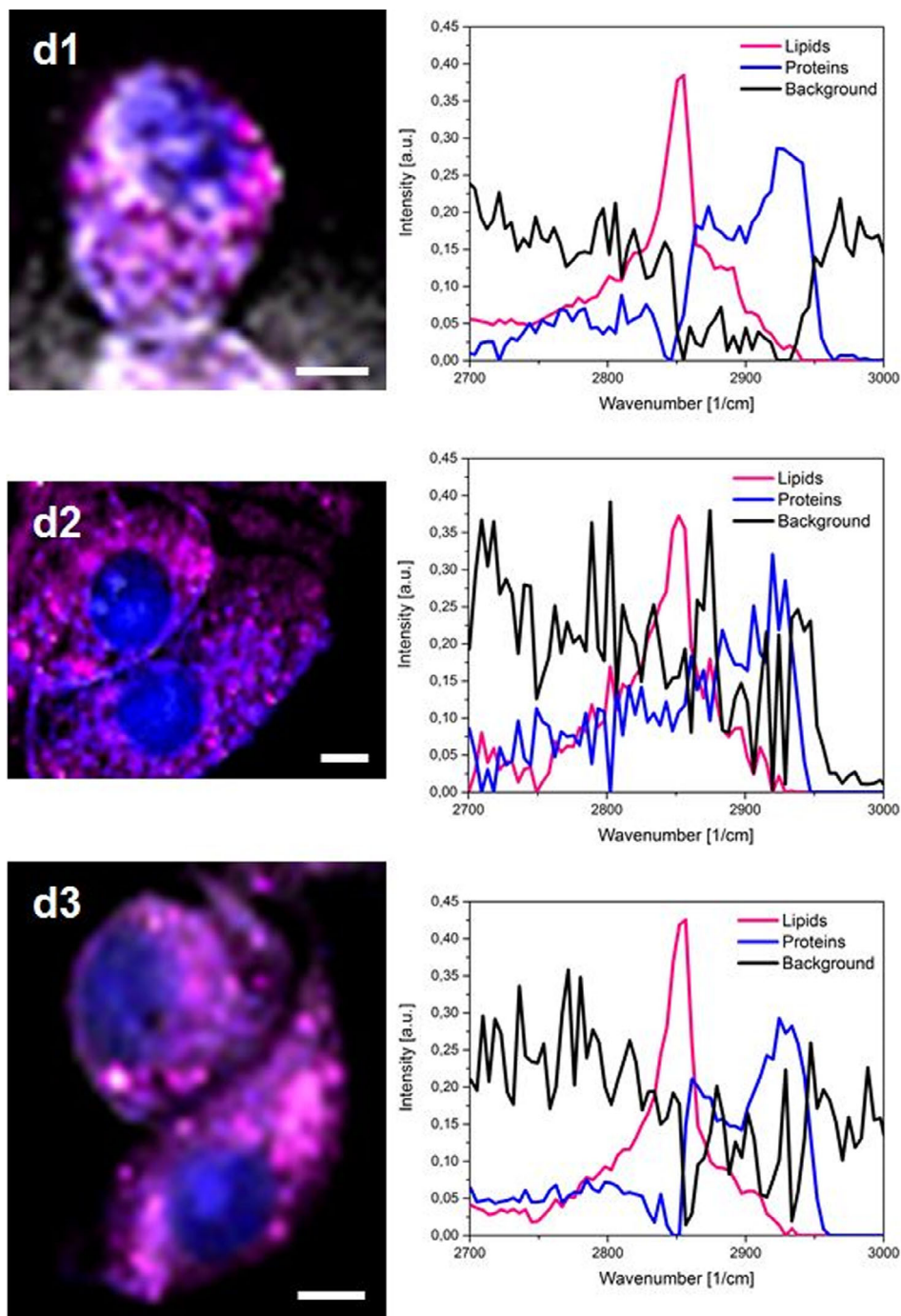
FIGURE 4 Hyperspectral (HS) coherent anti-Stokes Raman scattering (CARS) overlay images of ATII cells at day 1, 2 and 3. False-color coding provided by nonnegative matrix factorization (NNMF) results: three individual channels are shown, representing the lipid rich environment depicted in pink; nuclei depicted in blue; background depicted in gray, respectively (scale bars 1 μm). On the right hand side the NNMF eigenvectors are shown, corresponding to the different spectral components in the images averaged over the entire image. We observe lipid droplet formation from day 1 to day 2. On day 3, the size and number of the lipid droplets further increases, while the cellular volume starts to increase
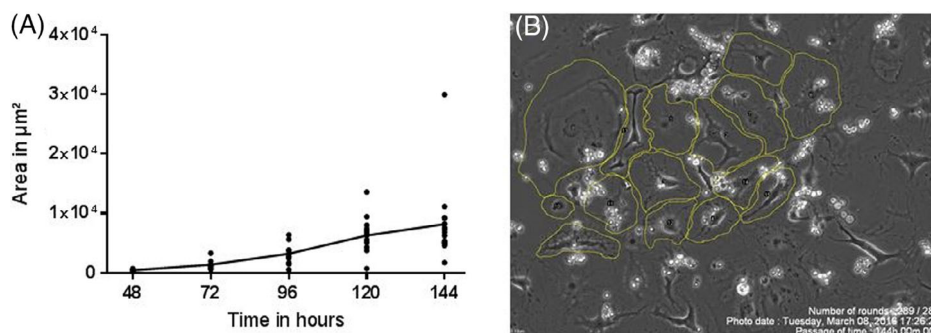
FIGURE 5 A, Cell surface area measurements of single alveolar epithelial cells at 48, 72, 96, 120 and 144 hours (n = 15 cells), acquired from the video data (Supplementary video 1). B, Video image at 144 hours, with marked cells used for surface measurements

differentiation of lipid rich vesicles (2845 cm^{-1}) from cellular proteins (2930 cm^{-1}) according to their vibrational signature (Figure S10). These data further corroborate the CRM experiments (Figure 4). Even though the special properties of ATI cells, that is, their exceedingly flat morphology, make it difficult to provide further distinguishing feature past day 3, several recent papers have demonstrated that CARS microscopy is well suited for following the differentiation of stem cells [32–35]. To observe the gradual metamorphosis of ATII into ATI-like cells on a larger scale, we finally performed live cell video imaging. Long-term observation during 6 days of incubation showed a very quick dynamic process of cellular growth and barrier formation. At day 1, ATII cells are small and cuboidal in shape; grouped together to form small islands. Over time, they flatten and spread out, while exhibiting a roughly circular, elevated, central perinuclear region, surrounded by cytoplasmic attenuations (Video S1). In addition, cell surface area measurements were performed by using the aforementioned video (Figure 5) elucidate rather linear increase of the cellular surface starting from 48 hours. The expanding rate was approximately 85 μm^2/hour in mean ($R^2 = 0.97$) calculated from 24 hours to 144 hours (n = 15 cells). However, a few cells showed nonlinear surface expansion due to the lack of neighboring cells. More precisely, alveolar epithelial cells need space to expand, nevertheless the interaction with neighbor cells seems to be a key role for cellular grow and further differentiation.

4 | CONCLUSIONS

In the present study, we aimed for label-free and nondestructive visualization of the gradual metamorphosis of primary human alveolar epithelial cells by applying confocal Raman and CARS microscopy. The chemically selective Raman spectra were successfully correlated to gradual morphological and molecular changes of the individual cells during their differentiation from ATII to ATI-like cells. The ATII phenotype was identified based on strong and localized phospholipid vibrations (specifically phosphatidyl choline). On the contrary, the ATI-like phenotype yielded spectra with

significantly less lipid content and absence of vesicular structures. Complementary, CARS microscopy allowed for a 3D visualization of alveolar surfactant rich vesicles within ATII cells and their secretion, with significantly improved z resolution. As the last step, HS CARS imaging combined the two major advantages of both methods. It enabled distinction between cellular proteins and lipids according to their vibrational signatures with acquisition times comparable with CARS, thus opening a new path for advanced label-free cellular investigation. This study does not only enrich the knowledge about human alveolar epithelial cells differentiation and the associated biomolecular changes, but also paves the path for further label-free investigations of lung cells and the role of the pulmonary surfactant on a molecular level. This knowledge can serve as a valuable basis for rational design of novel lung therapeutics.

CONFLICTS OF INTEREST

The authors have no conflicts of interest to report.

REFERENCES

[1] S. Fuchs, A. J. Hollins, M. Laue, U. F. Schaefer, K. Roemer, M. Gumbleton, C. M. Lehr, *Cell Tissue Res.* **2003**, *311*, 31.

[2] J. D. Crapo, B. E. Barry, P. Gehr, M. Bachofen, E. R. Weibel, *Am. Rev. Respir. Dis.* **1982**, *126*, 332.

[3] L. G. Dobbs, *Am. J. Physiol.* **1990**, *258*, L134.

[4] H. Fehrenbach, *Respir. Res.* **2001**, *2*, 33.

[5] B. D. Uhal, *Am. J. Physiol.* **1997**, *272*, L1031.

[6] J. M. Cheek, M. J. Evans, E. D. Crandall, *Exp. Cell Res.* **1989**, *184*, 375.

[7] L. Campbell, A. J. Hollins, A. Al-Eid, G. R. Newman, C. von Ruhland, M. Gumbleton, *Biochem. Biophys. Res. Commun.* **1999**, *262*, 744.

[8] F. Draux, C. Gobinet, J. Sule-Suso, A. Trussardi, M. Manfait, P. Jeannesson, G. D. Sockalingum, *Anal. Bioanal. Chem.* **2010**, *397*, 2727.

[9] J. W. Chan, D. S. Taylor, D. L. Thompson, *Biopolymers* **2009**, *91*, 132.

[10] S. R. Pygall, J. Whetstone, P. Timmins, C. D. Melia, *Adv. Drug Del. Rev.* **2007**, *59*, 1434.

[11] G. J. Puppels, F. F. de Mul, C. Otto, J. Greve, M. Robert-Nicoud, D. J. Arndt-Jovin, T. M. Jovin, *Nature* **1990**, *347*, 301.

[12] B. Kann, H. L. Offerhaus, M. Windbergs, C. Otto, *Adv. Drug Deliv. Rev.* **2015**, *89*, 71.

[13] I. Notingher, G. Jell, U. Lohbauer, V. Salih, L. L. Hench, *J. Cell. Biochem.* **2004**, *92*, 1180.

[14] J. W. Chan, D. S. Taylor, T. Zwerdling, S. M. Lane, K. Ihara, T. Huser, *Biophys. J.* **2006**, *90*, 648.

[15] I. Notingher, I. Bisson, A. E. Bishop, W. L. Randle, J. M. Polak, L. L. Hench, *Anal. Chem.* **2004**, *76*, 3185.

[16] J. X. Cheng, X. S. Xie, *Science* **2015**, *350*, aaa8870.

[17] M. Winterhalder, A. Zumbusch, *Adv. Drug Deliv. Rev.* **2015**, *89*, 135.

[18] N. Daum, A. Kuehn, S. Hein, U. F. Schaefer, H. Huwer, C. M. Lehr, *Methods Mol. Biol.* **2012**, *806*, 31.

[19] C. C. De Vequi-Suplicy, C. R. Benatti, M. T. Lamy, *J. Fluoresc.* **2006**, *16*, 431.

[20] T. Parasassi, G. De Stasio, A. d'Ubaldo, E. Gratton, *Biophys. J.* **1990**, *57*, 1179.

[21] T. Parasassi, G. De Stasio, G. Ravagnan, R. M. Rusch, E. Gratton, *Biophys. J.* **1991**, *60*, 179.

[22] T. A. Pologruto, B. L. Sabatini, K. Svoboda, *Biomed. Eng. Online* **2003**, *2*, 13.

[23] M. W. Berry, M. Browne, A. N. Langville, V. P. Pauca, R. J. Plemmons, *Comput. Stat. Data Anal.* **2007**, *52*, 155.

[24] D. S. Phelps, J. Floros, *Exp. Lung Res.* **1991**, *17*, 985.

[25] M. Kalina, R. J. Mason, J. M. Shannon, *Am. J. Respir. Cell Mol. Biol.* **1992**, *6*, 594.

[26] M. F. Beers, C. Y. Kim, C. Dodia, A. B. Fisher, *J. Biol. Chem.* **1994**, *269*, 20318.

[27] M. Kasper, T. Reimann, U. Hempel, K. W. Wenzel, A. Bierhaus, D. Schuh, V. Dimmer, G. Haroske, M. Muller, *Histochem. Cell Biol.* **1998**, *109*, 41.

[28] G. R. Newman, L. Campbell, C. von Ruhland, B. Jasani, M. Gumbleton, *Cell Tissue Res.* **1999**, *295*, 111.

[29] J. Perez-Gil, T. E. Weaver, *Physiology (Bethesda)* **2010**, *25*, 132.

[30] S. O. Konorov, H. G. Schulze, N. J. Caron, J. M. Piret, M. W. Blades, R. F. B. Turner, *J. Raman Spectrosc.* **2011**, *42*, 576.

[31] M. Okada, N. I. Smith, A. F. Palonpon, H. Endo, S. Kawata, M. Sodeoka, K. Fujita, *Proc. Natl. Acad. Sci. U. S. A.* **2012**, *109*, 28.

[32] A. D. Hofemeier, H. Hachmeister, C. Pilger, M. Schurmann, J. F. Greiner, L. Nolte, H. Sudhoff, C. Kaltschmidt, T. Huser, B. Kaltschmidt, *Sci. Rep.* **2016**, *6*, 26716.

[33] S. O. Konorov, C. H. Glover, J. M. Piret, J. Bryan, H. G. Schulze, M. W. Blades, R. F. B. Turner, *Anal. Chem.* **2007**, *79*, 7221.

[34] A. Downes, R. Mouras, P. Bagnaninchi, A. Elfick, *J. Raman Spec.* **2011**, *42*, 1864.

[35] Y. J. Lee, S. L. Vega, P. J. Patel, K. A. Aamer, P. V. Moghe, M. T. Cicerone, *Tissue Eng. Part C Methods* **2014**, *20*, 562.

SUPPORTING INFORMATION

Additional supporting information may be found online in the Supporting Information section at the end of this article.